# TRANSPORT PROPERTIES OF $Cu_2ZnSnS_4$

**M. Guc[1], K. G. Lisunov[2], A. Nateprov, S. Levcenko, V. Tezlevan, and E. Arushanov**

*Institute of Applied Physics, Academy of Sciences of Moldova, Academiei str. 5, Chisinau, MD-2028 Republic of Moldova*

[1]*e-mail: gmax@phys.asm.md*, [2] *kgl-official@rambler.ru*

(Received 16 December 2011)

## Abstract

Temperature dependence of the resistivity, $\rho(T)$, of five single crystalline p-$Cu_2ZnSnS_4$ samples is investigated in the interval of $T \sim 300–10$ K. Below ~200 K, $\rho(T)$ exhibits an activated behavior obeying the Mott variable-range hopping conductivity law between ~130–150 K and ~30–70 K. Analysis of the experimental data yields relative acceptor concentration values. In addition, the values of dielectric permittivity, width of the acceptor band, and density of the localized states are estimated.

## 1. Introduction

Recently, promising quaternary $Cu_2ZnSnS_4$ compound absorber layers have attracted considerable interest [1–8]. It is believed that these materials, due to their low cost and low-toxic and abundant elements [1], are alternative of more expensive $CuIn_{1-x}Ga_xSe_2$ thin-film solar cell absorber materials, showing at present a high conversion efficiency of ~20 % [2]. Thin-film solar cells of $Cu_2ZnSnS_4$ with efficiency exceeding 9% have been fabricated so far [3]. This compound is also interesting as a wide-gap *p*-type thermoelectric material [8] as well as a photoelectrode for $H_2$ evolution from water [9–11].

$Cu_2ZnSnS_4$ crystallizes into two different structures, kesterite with space group $I\bar{4}$ and stannite (space group $I\bar{4}2m$) modifications, having 4 Cu, 2 Zn, 2 Sn, and 8 S atoms per unit cell and differing by 4 and 3 inequivalent bonds of S atoms, respectively [12, 13]. On the other hand, the disordered (mixed) structure has been observed as well [13, 14]. The point is that the total energies of both modifications are found to be very close, which favors the formation of a disordered structure with a more random distribution of Cu and Zn on cation positions, although the kesterite structure has a lower energy [13].

First-principles calculations of the electronic structure [13] and of a series of intrinsic defects and defect complexes [15], as well as investigations of the phase stability and defect formation in $Cu_2ZnSnS_4$ [16], were performed. The effective electron and hole masses, the fundamental band gap energy and high-frequency dielectric constant, $\kappa_\infty$, were evaluated. Namely, for holes of the topmost valence band, the transversal effective mass values of $m_\perp = 0.71$ and 0.33 and the longitudinal effective mass values of $m_\parallel = 0.22$ and 0.84, for kesterite and stannite structures, respectively, were obtained (in units of free electron mass, $m_0$) [13]. Those of $\kappa_\infty$ ranging from 6.5 to 7.1 were found to be less anisotropic and having closer values for both modifications of $Cu_2ZnSnS_4$ [13].

Photoluminescence of $Cu_2ZnSnS_4$ single crystals [17, 18] and films [19] was studied. Defect recombination model with a shallow donor below the conduction band (~ 5 meV) and two

shallow acceptors above the valence band, with energies $E_1 = 10 \pm 5$ meV and $E_2 \approx 30 \pm 5$ meV, was proposed [18]. Assuming an exciton binding energy of 10 meV, the value of the band gap $E_g = 1.519$ eV at 10 K was found [18].

The transport properties of $Cu_2ZnSnS_4$ polycrystalline thin films were investigated [4–7, 19], establishing the *p*-type conductivity but concentrating mainly on the resistivity data in the interval around the room temperature. On the other hand, the expected high degree of the microscopic lattice disorder favours a hopping charge transfer, which makes it important to study the low-temperature conductivity of the single-crystalline material.

Here, we present the resistivity measurements of p-$Cu_2ZnSnS_4$ single crystals in the temperature interval between 10–300 K and the analysis of low-temperature resistivity data. The purpose of the work is to investigate the hopping conductivity of the compound and to determine the microscopic properties of the localized carriers as well as some important macroscopic parameters of p-$Cu_2ZnSnS_4$.

## 2. Experimental

Single crystals of $Cu_2ZnSnS_4$ were grown by chemical vapor transport using iodine as a transport agent. The grown process was done in an evacuated quartz horizontal ampoule from the stoichiometric melt of high-purity precursors Cu, Zn, Sn, and S. The evaporation temperature was kept at 850$^o$ C, the grown temperature was 800$^o$ C, and the concentration of iodine was 5 mg/cm$^3$. The energy dispersive X-ray microanalysis (EDX) was used to analyze the degree of stoichiometry of the investigated crystals. EDX measurements yield a slight excess of Sn and S, the composition ratios being Cu/(Zn + Sn) ≈ 0.98, Zn/Sn ≈ 0.86, S/metals ≈ 1.045. All crystals exhibited *p*-type conductivity. The difference in composition ratio of samples studied is about 3% corresponding to the accuracy of our EDX measurements.

Resistivity, ρ (*T*), was measured using the van der Pauw method in a range of 10–300 K. The contacts were made with a silver paste, and the results do not depend on surface treatment. It is evident from Fig. 1 that all the investigated p-$Cu_2ZnSnS_4$ samples exhibit an activated conductivity below $T \sim 200$ K.

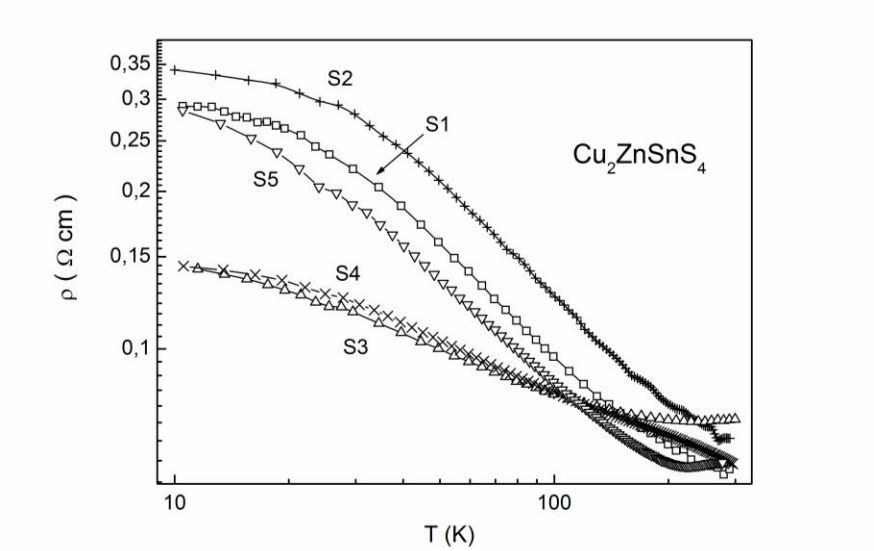


**Fig. 1.** Temperature dependence of the resistivity in the investigated samples S1– S5.

## 3. Theoretical background

A detailed analysis of the low-temperature data in Fig. 1 is performed using a universal expression for the resistivity of weakly doped crystalline semiconductors in the domain of the hopping charge transfer [20, 21]:

$$\rho(T) = A_p T^m \exp\left[\left(\frac{T_{0p}}{T}\right)^{1/p}\right]. \quad (1)$$

Here $A_p$ is the prefactor constant, $p = 1$ refers to hopping over only the nearest-neighboring sites or the NNH conductivity, $p = 4$ describes the Mott type of the variable-range hopping (VRH) conductivity regime, $p = 2$ the Shklovskii-Efros VRH conduction mechanism, $T_{0p}$ is the characteristic hopping temperature and $m = 1/p$ [21]. Transition from the NNH to the VRH conduction regime takes place when it becomes energetically favorable for electrons to jump beyond the nearest-neighboring sites [20, 21]. This situation is usually stimulated by lowering the temperature or increasing the microscopic disorder [20, 21]. The Mott VRH regime takes place in the case where the electron correlation effects can be neglected, resulting in a constant nonzero value, $g$ (μ), of the density of the localized states (DOS) around the Fermi level, μ [20]. The Shklovskii-Efros VRH conduction sets in the case where the Coulomb interactions between the electrons become important and lead to a parabolic dependence of the DOS, $g$ (ε) ~ (ε – μ)$^2$, within an energy interval of the Coulomb gap, (μ – Δ, μ + Δ) [21]. The higher ratio of Δ/$W$, where $W$ is half width of the impurity band (for briefness, below it is referred to simply as "width of the band"), implies the increased importance of the Coulomb correlations and stimulates the onset of the Shklovskii-Efros VRH conduction at higher temperatures.

The characteristic temperature at $p = 1$ is written usually as $T_{01} = E_{act} / k$, where $E_{act}$ is the NNH activation energy, whereas for the VRH conductivity ($p = 4$ and 2) the expressions

$$T_{04} = \frac{\beta_4}{kg(\mu)a^3} \quad \text{and} \quad T_{02} = \frac{\beta_2 e^2}{\kappa k a} \quad (2)$$

are valid, respectively. In Eq. (2) $\beta_4 = 21$ and $\beta_2 = 2.8$ are numerical constants, $\kappa$ is the dielectric permittivity, and $a$ is the localization radius of charge carriers [21], which is sensitive to proximity to the metal-insulator transition (MIT). This is given by the expression

$$a = a_0 (1 - N/N_c)^{-\nu}, \quad (3)$$

where $a_0$ is the localization radius far from the MIT, $\nu \approx 1$ is a critical exponent, $N$ is the concentration of sites involved in the hopping (acceptors in the case of p-$Cu_2ZnSnS_4$), and $N_c$ is the critical concentration of the MIT [22]. Parameters $a_0$ and $N_c$ are interrelated with the Mott universal criterion [20]:

$$N_c^{1/3} a_0 \approx 0.25. \quad (4)$$

At this point, it is important to mention another expression describing proximity of a system to the MIT:

$$a \sim | \mu - E_c |^{-\nu}, \quad (3')$$

which is referred to as the Anderson MIT in the impurity band with coexisting localized and extended states separated by the mobility threshold, $E_c$ [20].

The type of the hopping conductivity can be determined with Eq. (1) by linearization of ρ ($T$) in coordinates of ln ($\rho T^{-1/p}$) vs. $T^{-1/p}$ or analyzing the local activation energy [21]:

$$E_{loc}(T) = \frac{d[\ln \rho(T)]}{d(kT)^{-1}}. \quad (5)$$

Introducing $E_{loc}$ ($T$), Eq. (1) can be presented in the following form

$$\ln[E_{loc}/(kT)+m] = \ln(1/p) + (1/p)\ln T_{0p} + (1/p)\ln(1/T), \quad (6)$$

where $m = 1/p$ [see remarks to Eq. (1)]. Namely, by putting $m$ = 1, 1/2 or 1/4 in the left-hand side of Eq. (6), from the linear part of the plots of $\ln[E_{loc}/(kT) + m]$ vs. $\ln(1/T)$ one should obtain $p$ = 1, 2 or 4, respectively, provided that one of the above discussed three hopping conduction regimes takes place.

## 4. Analysis and discussion

### 4.1. Identification of the conductivity mechanism

Using at first the method of linearization of ρ ($T$) with Eq. (1) and taking different tentative values of $p$ = 1, 4, and 2, we find the best linearity of the plots shown in Fig. 2 implying that $p$ = 4 and the Mott VRH conductivity is established unambiguously in all the investigated samples. The linear fit of the plots in Fig. 2 yields the values of $A_4$ and $T_{04}$, as well as those of $T_v$ and $T_m$ (the onset and the lowest temperature of the Mott VRH conduction interval, respectively), which are listed in Table 1.

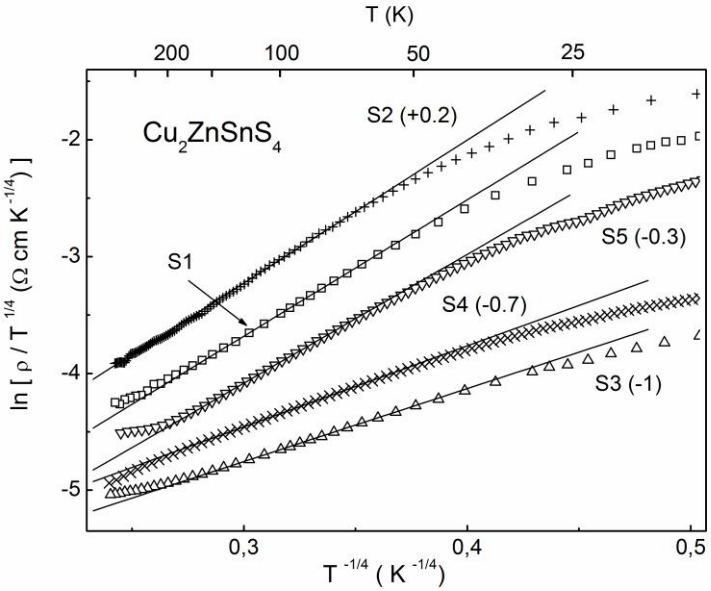


**Fig. 2.** Plots of ln ($\rho/T^{1/4}$) vs. $T^{-1/4}$ for the investigated samples S1– S5. For convenienc, the plots for samples S2 – S5 are shifted along the vertical axis by the values shown in parenthesis. The straight lines are linear fits.

Figure 3 shows that the Mott regime of the VRH conduction is supported by the plots of ln [ $E_{loc}/(kT)$ + 1/4 ] vs. ln 1/$T$ for samples S1, S4 and S5. The straight lines are drawn for $p$ = 4 yielding the values of $T_0 \approx 19.2\times10^4$, $2.28\times10^3$, and $1.47\times10^4$ K; $T_v \approx$ 122, 133, and 145 K; and $T_m \approx$ 63, 68, and 85 K for samples S1, S4, and S5, respectively, which are very close to the respective data in Table 1. It is important to mention that the strong variation of the values of $T_{04}$ in our samples is attributed, according to Eqs. (2) and (3), to a proximity to the MIT rather than to large variation of $g$ (μ). In fact, if $N$ is close to $N_c$, only a small scattering of $N$ can cause an appreciable variation of $a$ and lead to the large scattering of $T_{04} \sim a^{-3}$. On the other hand, strong

changes of $g$ (μ) in the samples obtained with the same preparation method are unlikely.

**Table 1.** Prefactor constant ($A_4$), the onset ($T_v$) and lowest ($T_m$) temperatures of the Mott VRH conduction regime, the Mott VRH characteristic temperature ($T_{04}$) and the bandwidth parameter ($W_0$) of the investigated p-$Cu_2ZnSnS_4$ samples

| Sample No. | $A_4$ ($\Omega$ cm $K^{-1/4}$) | $T_v$ (K) | $T_m$ (K) | $T_{04}$ (K) | $W_0$ (meV) |
|---|---|---|---|---|---|
| 1 | $7.60\times10^{-4}$ | 130 | 50 | $1.86\times10^{4}$ | 38.6 |
| 2 | $8.29\times10^{-4}$ | 150 | 55 | $2.24\times10^{4}$ | 45.1 |
| 3 | $3.59\times10^{-3}$ | 133 | 32 | $1.52\times10^{3}$ | 21.0 |
| 4 | $2.92\times10^{-3}$ | 132 | 65 | $2.31\times10^{3}$ | 23.2 |
| 5 | $8.31\times10^{-4}$ | 151 | 77 | $1.48\times10^{4}$ | 40.9 |

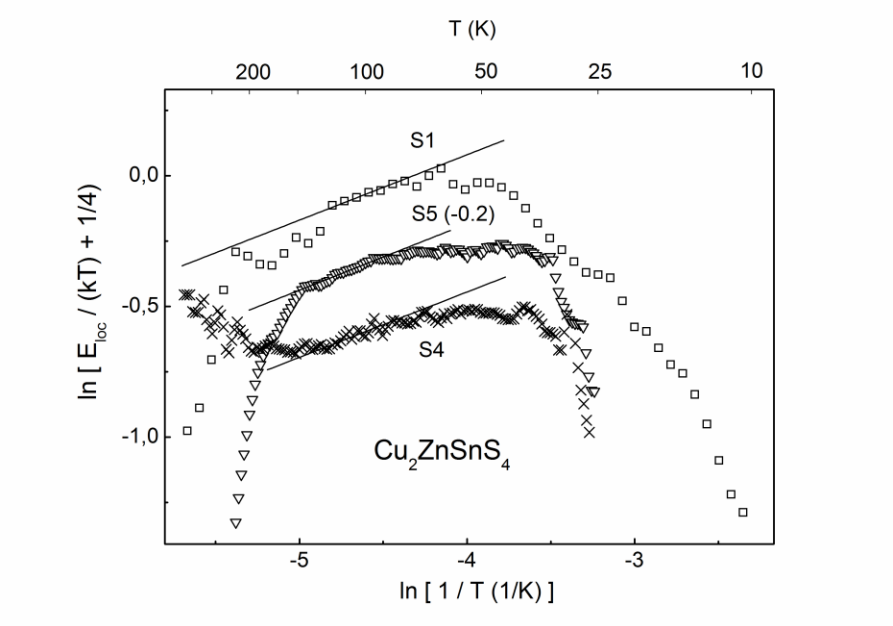


**Fig. 3.** Plots of ln [$E_{loc}$ / (kT) + 1/4] vs. ln (1/T) for samples S1, S4, and S5. The plot for S4 is shifted by − 0.2 units along the vertical axis for convenience. The straight lines correspond to the constant slope of 1/p = ¼.

### 4.2. Model of the acceptor band

An important parameter $W_0 = k\,(T_v^3 T_{04})^{1/4}$ connected to the width of the impurity band, $W$, is exhibited in Table 1, as well. In fact, as shown by Mott [20], the VRH conduction takes place within an optimum energy stripe (μ – $E_M$, μ + $E_M$), where the Mott energy is given by the relation $E_M(T) = kT\,\xi_c(T)$ and the percolation threshold for the Mott VRH regime by the expression $\xi_c(T) = (T_{04}/T)^{1/4}$ [21]. Hence, at the onset VRH temperature, $T_v$, one finds

$E_M$ ($T_v$) = $k$ ($T_v^3 T_{04}$)$^{1/4}$ = $W_0$. On the other hand, a criterion of transition to the Mott VRH conduction at $T = T_v$ can be written as $<\Delta E> \approx <\Delta E_M>$, where $<\Delta E>$ is the mean difference of the electron energy during hopping and $<\Delta E_M>$ is the mean difference of the electron energy within the Mott optimum stripe. Suppose first a case of intermediate degree of the compensation, $K \sim 1/2$, when $\mu$ is lying close to the center of the impurity band. Then one finds $<\Delta E> \approx 1/2\ (2W) \approx W$, $<\Delta E_M> \approx 1/2\ (2E_M) \approx E_M$, and the criterion above leads at $T = T_v$ to the relation $W\,|_{K \sim 1/2} \approx W_0$ [21]. On the other hand, for the case of a weak compensation, $K << 1$, $\mu$ lies close to the band edge, $\mu = W - \delta$, which gives similarly: $<\Delta E> \approx W + \delta/2$, $<\Delta E_M> \approx E_M/2 + \delta/2$ and $W\,|_{K << 1} \approx W_0/2$, provided that $\delta << W_0$. Above we take into account that, for $K << 1$, almost half of the Mott optimum stripe lies outside the impurity band, which has a definite sense if the band can be characterized with clear-cut edges (e.g., this is strictly substantiated for the rectangular DOS shape).

Hence, it follows from Table 1 that the typical width of the acceptor band in our samples, expected to lie between $W \sim W_0/2$ and $W_0$ (depending on $K$), is comparable with the values of the acceptor levels, $E_1 \approx 10$ meV and $E_2 \approx 30$ meV found in $Cu_2ZnSnS_4$ [18] (see Introduction). This implies a high microscopic disorder in the investigated samples and a strong broadening of the acceptor levels $E_1$ and $E_2$ into the wide acceptor bands, where the band widths should be connected mainly to disorder. Under these conditions, these bands are strongly overlapped, and it is reasonable to treat them as a single band, as shown in the left panel of Fig. 4. Then the energy of the peak or center of the unified band can be found approximately as $E_0 \approx (E_1 + E_2)/2 \approx 20$ meV.

Next, the resulting broad band under conditions of proximity to the MIT should possess also a wide interval of extended states around the center and two intervals of the localized states shifted to the band edges or tails [20], as shown schematically in the right panel of Fig. 4 where the localized states are hatched. Therefore, the position of $\mu$ near the center of the band and an intermediate degree of the compensation can be excluded in our case, otherwise the activated conduction would not be observed. On the other hand, strong compensation and position of $\mu$ near the left-hand band edge in Fig. 4 are unlikely, because proximity to the MIT means a closeness of $\mu$ to the left mobility edge, $-E_c$. However, in this case, the interval ($-E_c$, $E_c$) of the extended states at $T = 0$ would be free of holes, which suggests that, at low temperatures, there occurs a strong domination of the conduction, connected to activation of the holes into the interval ($-E_c$, $E_c$) rather than hopping charge transfer [20]. This type of conductivity yields the dependence of $\rho(T)$ differing considerably from the Mott VRH conduction but resembling the NNH conduction [20], where $p = 1$, and $E_{act} = |\mu - E_c|$ in Eq. (1) would be very small, strongly stimulating this type of conductivity. Since no signs of this mechanism is observed in our case, it is reasonable to suppose that $K << 1$ and $\mu$ lies inside the right-hand interval of the localized states, as shown in the right of Fig. 4. To proceed further and obtain important numerical results, we approximate the DOS of the acceptor band with a rectangular shape shown by the dashed line in the right panel of Fig. 4. This considerably simplifies the subsequent analysis but brings an additional error discussed later. Eventually, we neglect $\delta$ and put $\mu \approx W \approx W_0/2$ in the numerical analysis below.

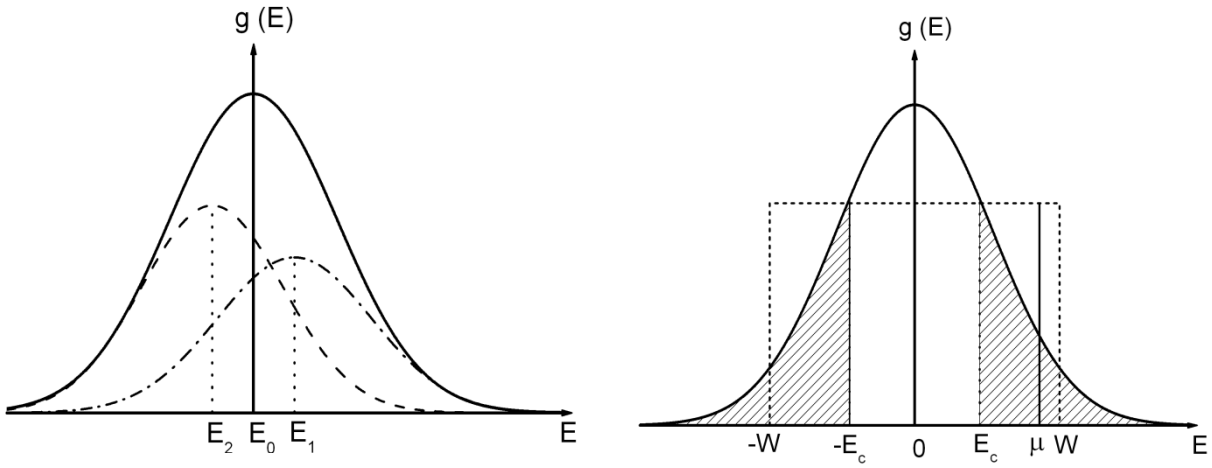


**Fig. 4.** Left panel: plots of g (E) for two strongly overlapped impurity bands with peaks at energies $E_1$ (dash-dot line) and $E_2$ (solid line). The solid line represents the plot of DOS vs. energy of the unified impurity band having a peak at $E_0$ (schematically). Right panel: image of DOS vs. energy of the unified band containing the extended states between the mobility edges – $E_c$ and $E_c$ and the localized states outside them, shown by the hatched area (solid line). The dashed line represents the approximation of the DOS with a rectangular shape (schematically).

### 4.3. Numerical analysis of the temperature parameters

Using (1), (3), and (4), putting $g(\mu) \approx N/(2W)$, where $W \approx W_0/2 \approx (1/2)k\,(T_v^{\,3}T_{04})^{1/4}$, we find the equation

$$\left(\frac{T_{04}}{T_v}\right)^{1/4} \approx 4\beta_4^{1/3}\left(\frac{N}{N_c}\right)^{1/3}\left(1-\frac{N}{N_c}\right)^{\nu}, \qquad (7)$$

which yields, at $\nu \approx 1$ and with the data of $T_{04}$ and $T_v$ in Table 1, the values of the $N/N_c$ ratio and those of $a/a_0$ listed in Table 2. The values of $N/N_c \sim 0.72$–$0.84$ and $a/a_0$, which were found with $N/N_c$ and Eq. (3) at $\nu \approx 1$ and lying appreciably above unity (Table 2), are consistent with proximity of the acceptor system in the investigated samples to the MIT, as has been supposed above.

**Table 2.** Localization radius in units of that far from the MIT ($a/a_0$) and in units of the Bohr radius ($a/a_B$), the relative acceptor concentration ($N/N_c$), the width of the acceptor band (W), the mobility threshold ($E_c$) and the DOS (g (μ)) in the investigated p-$Cu_2ZnSnS_4$ samples

| Sample No. | $a/a_0$ | $a/a_B$ | $N/N_c$ | $W$ (meV) | $E_c$ (meV) | $g(\mu)$ ($10^{16}$ mev$^{-1}$cm$^{-3}$) |
|---|---|---|---|---|---|---|
| 1 | 3.6 | 3.9 | 0.72 | 19.3 | 15.4 | 4.1 |
| 2 | 3.5 | 3.2 | 0.72 | 22.5 | 17.2 | 3.5 |
| 3 | 6.4 | 8.9 | 0.84 | 10.5 | 9.5 | 8.8 |
| 4 | 5.8 | 7.8 | 0.83 | 11.6 | 10.3 | 7.9 |
| 5 | 3.9 | 3.7 | 0.74 | 20.4 | 16.1 | 4.0 |

The value of $a_0 \approx \hbar/(2mE_0)^{1/2}$ [21] can be calculated approximately by putting $E_0 \approx 20$ meV (see *Section 4.2*) and treating $m$ as a mean effective mass of the holes, $m \approx \left(m_\perp^2 m_\parallel\right)^{1/3}$ [21]. Using the data of $m_\perp$ and $m_\parallel$ in $Cu_2ZnSnS_4$ [13] (see Introduction), we find $m = 0.47 \pm 0.02$; that is, for both modifications of $Cu_2ZnSnS_4$, $m$ is varied insignificantly, which yields $a_0 \approx 20$ Å.

On the other hand, the relation $a_0 \approx a_B$ is fulfilled for shallow hydrogen-like impurity levels [20, 21], where

$$a_B = \hbar^2\kappa_0/(me^2) \tag{8}$$

is the Bohr radius and $\kappa_0$ is the static dielectric permittivity far from the MIT. Therefore, the $a/a_B \approx a/a_0$ ratio can be calculated independently with Eq. (3'), written in the form

$$a/a_B \approx (\mu/E_c - 1)^{-\nu}, \tag{9}$$

putting $\nu \approx 1$, $\mu \approx W \approx W_0/2$ (*see Section 4.2*) and using the expression [20]

$$E_c \approx W - \frac{V_0^2}{4(z-1)J}. \tag{10}$$

In Eq. (10) $z \approx 6$ is the number of nearest neighbors in the acceptor system, $V_0$ represents a scale of scattering of the hole energy due to the microscopic disorder [20], and $J = J_0 \exp(-R/a_B)$ is the overlap integral. Here $R \approx (4\pi N/3)^{-1/3}$ is half of the mean distance between the acceptors, and the prefactor $J_0$ can be written as

$$J_0 \approx \frac{e^2}{\kappa_0 a_B}\left[\frac{3}{2}\left(1+\frac{R}{a_B}\right)+\frac{1}{6}\left(\frac{R}{a_B}\right)^2\right], \tag{11}$$

similar to [20] but differing by the introduction of $\kappa_0$ in the denominator of Eq. (11). This modification of the original expression of Eq. (11) is important, because a system of disordered sites in vacuum was considered in [20], whereas a corresponding system of impurity sites in semiconductors exists in media of the host lattice [21]. Eventually, taking into account the presumed main reason for broadening of the acceptor states into the acceptor bands connected to the lattice disorder (see *Section 4.2*), one can put $V_0 \approx 2W \approx W_0$ [20]. Hence, we can evaluate the ratio of $a/a_B$ with Eqs. (8–11) using a single adjustable parameter, $\kappa_0$, to fit $a/a_B$ to the data of $a/a_0$ in Table 2 by minimizing the standard deviation.

However, an important detail should be discussed preliminary. It follows from Tables 1 and 2 that the values of $W$ in samples S3 and S4 are ~2 times lower than in S1, S2, and S5, whereas $2W \approx W_0$ is close to the difference of $E_2 - E_1 \approx 20$ meV. This means that the overlap of the bands generated by broadening of the levels $E_2$ and $E_1$ is appreciably smaller in S3 and S4, which worsens the applicability of our model of a single acceptor band to these samples and makes the fitting procedure less accurate in the case where the data of these samples are involved.

Therefore, at first, we fit the values of $a/a_0$ with $a/a_B$ only for samples S1, S2, and S5, yielding $\kappa_0 \approx 17$, $a_B \approx 19$ Å, $E_B \approx 22$ meV, and $E_H \approx 27$ meV, where $E_B = \hbar^2/(2ma_B^2)$ and $E_H \approx 5e^2/(8\kappa_0 a_B)$ are the Bohr energy and the Hubbard on-site correlation energy of the shallow hydrogen-like impurity, respectively [20, 21]. The values of $a/a_B$ calculated with Eq. (9) are displayed in Table 2 as well as those of $E_c$ evaluated with Eq. (10). We can see a reasonable agreement between $a/a_0$ and $a/a_B$ in S1, S2, and S5, which is worsening for S3 and S4 as can be expected from the preliminary discussion above. Next, $N_c$ can be found with the Mott criterion, $N_c^{1/3}a_B \approx 0.25$, which gives $N_c \approx 2.2\times10^{18}$ cm$^{-3}$. Eventually, the data of $N/N_c$ from Table 2 yield those of $N$ and the values of $W$ from Table 2 permits the evaluation of $g(\mu) \approx N/(2W)$, which is shown in Table 2.

In the case where all the data of $a/a_0$ in Table 2 are involved in the fitting with $a/a_B$, we find $\kappa_0 \approx 19$, $a_B \approx 22$ Å, $E_B \approx 18$ meV and $E_H \approx 22$ meV. The parameters $a/a_B$, $E_c$, $N_c$ and $g$ ($\mu$) are comparable with the corresponding previous data. On the other hand, now $E_B$, representing the centre of the acceptor band, is found to be systematically smaller than $W$ in samples S1, S2, and S5 (Table 5), which however are expected to follow better the model formulated in *Section 4.2*. This issue is in line with the preliminary discussion above. Therefore, the numerical values of the parameters obtained by fitting of $a/a_0$ only for S1, S2, and S5 look preferable.

### 4.4. Discussion

First of all, we should mention the proximity of $E_0 \approx 20$ meV guessed in *Section 4.2* and $a_0 \approx 20$ Å connected to $E_0$ (see *Section 4.3*) with those of $E_B \approx 22$ meV and $a_B \approx 19$ Å, respectively, evaluated within a more strict procedure above. Next, we pay attention to the similarity of $E_H \approx 27$ meV and the difference of $E_2 - E_1 \approx 20$ meV. The latter points out a possible nature of the two acceptor bands centered at $E_1$ and $E_2$ in $Cu_2ZnSnS_4$ as Hubbard-like bands. These bands appear via spin-splitting of the acceptor level due to the Hubbard correlation or repulsion of two holes with opposite spins localized on the same level [20]. However, broadening of these bands should be attributed mainly to the microscopic disorder rather than to an overlap of acceptor states. This can also be substantiated in another way. In fact, using the expressions of $E_B$ and $E_H$ at the end of *Section 4.3*, taking into account the relations $E_1 = E_B - E_H/2$ and $E_2 = E_B + E_H/2$, we find that $E_1 \approx E_B\,(1 - 5/8) \approx 8$ meV and $E_2 \approx E_B\,(1 + 5/8) \approx 35$ meV, where only the results of the present work (i.e., the above value of $E_B$) were used. Hence, it is evident that our values of $E_1$ and $E_2$ almost coincide with $E_1 = 10 \pm 5$ meV and $E_2 = 30 \pm 5$ meV found in [18], which makes it quite probable to regard the two acceptor bands in $Cu_2ZnSnS_4$ as Hubbard-like bands. At this point, the relation $E_0 \approx (E_1 + E_2)/2$ utilized in *Section 4.2* acquires a more strict meaning.

Concerning the applicability of the rectangular approximation of the DOS (right panel in Fig. 4) in general, it is supported by broadness of the acceptor band but is worsened by the position of $\mu$ close to the band edge. In fact, it is evident from the right panel of Fig. 4 that $g(\mu)$ can be appreciably smaller for a more realistic DOS (shown schematically with the solid line) than for the rectangular DOS (dashed line). At this point, the values of $g(\mu)$ found here should be regarded rather as some typical or mean values characterizing the acceptor band of strongly disordered $Cu_2ZnSnS_4$. Similar inference looks reasonable with respect to the values of $N/N_c$ and $a/a_0$, which are interrelated. However, their uncertainty should be evidently smaller than that of $g(\mu)$ above, because Eq. (2), which is important for the analysis, yields $T_{04} \sim [g\ (\mu)]^{-1}$ but $T_{04} \sim a^{-3}$. This considerably reduces the error of $a$ caused by the rectangular approximation of the DOS as well as the error of the other parameters obtained by fitting of $a/a_0$ with $a/a_B$. At this point, the validity of $E_B$ and $a_B$ being close to $E_0$ and $a_0$, respectively, has been already estimated above. The obtained value of $\kappa_0$ requires an independent substantiation, which is better to perform through optical measurements. Here we can only mention that $\kappa_0$ looks reasonable obeying the expected relation of $\kappa_0 > \kappa_\infty$ (see Introduction).

Finally, we discuss deviations of $\rho(T)$ from the Mott behavior visible in Fig. 2 and especially in Fig. 3. The high-temperature deviation is attributable to the NNH conductivity or to the band conduction connected to the thermal excitation of the holes into the valence band. Due to the relatively large value of $E_B$ or $E_0$ the first out of these reasons looks preferable, although the final conclusion at this point requires further substantiation. On the other hand, it is well

known that, in many doped semiconductors, the violation of the Mott VRH conduction regime with lowering $T$ is attributed to the onset of the Shklovskii-Efros VRH conductivity [22–24]. However, this should lead to the formation of the second slope, with $p = 1/2$, of the plots in Fig. 3, which is not observed down to at least ~25 K in S4 and S5 and down to 10 K in S1. At this point, it is possible to estimate the onset temperature of the Shklovskii-Efros behavior of $\rho(T)$ as follows. The value of the Coulomb gap can be obtained through the expression $\Delta \approx e^2/(\kappa R_A)$ [21], where $\kappa \approx \kappa_0 \ (a/a_0)^2$ [22] and $R_A = 2R$ is the mean distance between the acceptors, yielding $\Delta \approx 0.2 - 0.6$ meV. Hence, the low value of the $\Delta/W$ ratio shifts the onset of the Shklovskii-Efros VRH conduction regime to low temperature $T_{v2}$, which can be obtained with the expression $\Delta \approx 0.5\, k\, (T_{v2}\, T_{02})^{1/2}$ [21], where $T_{02}$ can be evaluated with the second of Eqs. (2). Eventually, we find $T_{v2} \approx 4–7$ K lying below the lowest temperature of 10 K used in this work. This suggests a broad intermediate interval, where both VRH conduction mechanisms make a comparable contribution to $\rho(T)$, which therefore cannot be characterized by Eq. (1) with any definite value of $p$.

## 5. Conclusions

We have studied the low-temperature conductivity of p-$Cu_2ZnSnS_4$ single crystals. The Mott variable-range hopping conduction is established within a broad temperature interval. Analysis of the resistivity data under conditions of the proximity to the Anderson metal-insulator transition and presumed low degree of compensation has yielded typical values of width of the acceptor band, the acceptor concentration, and the density of the localized states in the acceptor band as well as the localization and the Bohr radii of the holes and the dielectric permittivity far from the MIT. The results give evidence for a high degree of microscopic disorder in the studied p-$Cu_2ZnSnS_4$ samples.

## Acknowledgments

Financial supports from STCU # *5402* and from IRSES PVICOKEST – 269167 projects are acknowledged.

## References

[1] J.J. Scragg, P.J. Dale, L.M. Peter, G. Zoppi, and I. Forbes, Phys. Stat. Sol. b 245, 1772 (2008).
[2] I. Repins, M.A. Contreras, B. Egaas., C. DeHart, J. Scharf, C.L. Perkins, B. To, and R. Noufi, Prog. Photovolt. Res. Appl. 16, 235 (2008).
[3] T.K. Todorov, K.B. Reuter, and D.B. Mitzi, Adv. Mater. 22, 1 (2010).
[4] H. Kataghiri, N. Ishigaki, T. Ishida, and K. Saito, Jpn. J. Apl. Phys. 40, 500 (2001).
[5] Y. Kumar, G. Babu, P. Bhaskar, and V. Raja, Sol. Energ. Mat. Sol. C. 93, 1230 (2009).
[6] Y.B. Kumar, P. Bhaskar, G. Babu, and V. Raja, Phys. Stat. Sol. a 207, 149 (2010).
[7] J. Seol, S. Lee, J. Lee, H. Nam, and K. Kim, Sol. Energ. Mat. Sol. C. 75, 155 (2003).
[8] M.-L. Liu, Fu-Q. Huang, Li-D. Chen, and I-W. Chen, Appl. Phys. Lett 94, 202103 (2009).
[9] I. Tsuji, Y. Shimodaira, H. Kato, H. Kobayashi, and A. Kudo, Chem. Mater. 22, 1402 (2010).
[10] S. Ikeda, T. Nakamura, T. Harada, and M. Matsumura, Phys. Chem. Chem. Phys. 12, 13943 (2010).
[11] D. Yokoyama, T. Minegishi, K. Jimbo, T. Hisatomi, G. Ma, M. Katayama, J. Kubota, H.

Katagiri, and K. Domen, Appl. Phys. Express 3, 101202 (2010).
[12] S. Schorr, H.-J. Hoebler, and M. Tovar, Eur. J. Mineral. 19, 65 (2007).
[13] C. Persson, J. Appl. Phys. 107, 053710 (2010).
[14] S. Schorr, Thin Solid Films 515, 5985 (2007).
[15] S. Chen, X.G. Gong, A. Walsh, and Su-H. Wei, Applied Physics Letters 96, 021902 (2010).
[16] A. Nagoya, R. Asahi, R. Wahl, and G. Kresse, Phys. Rev. B 81, 113202 (2010).
[17] K. Tanaka, Y. Miyamoto, H. Uchiki, K. Nakazawa, and H. Araki, Phys. Stat. Sol. a 203, 2891 (2006).
[18] Hönes K., Zscherpel E., Scragg J., and Siebentritt S., Physica B: Condens. Matter 404, 4949 (2009)
[19] J.P. Leitao, N.M. Santos, P.A. Fernandes, P.M. Salome, A.F. P da Cunha, J.C. Gonzalez, G.M. Ribeiro, and F.M. Matinaga, Phys. Rev. B 84, 024120 (2011).
[20] N. Mott and E.A.Davies, Electron Processes in Non-Crystalline Materials, Clarendon, Oxford, 1979; Mott N. F., Metal–Insulator Transitions, Taylor and Francis, London, 1990.
[21] B.I. Shklovskii, and A.L. Efros, Electronic Properties of Doped Semiconductors, Springer, Berlin, 1984.
[22] T.G. Castner, Hopping Transport in Solids, Ed. M. Pollak and B. Shklovskii, North-Holland, Amsterdam, p 3, 1991.
[23] E. Arushanov, K.G. Lisunov, H. Vinzelberg, G. Behr, J. Schumann, and O. Schmidt, J. Appl. Phys. 104, 053720 (2008).
[24] K.G. Lisunov, H. Vinzelberg, E. Arushanov, and J. Schumann, Semicond. Sci. Technol. 26, 095001 (2011).